Glycine Adsorption at Nonstoichiometric (010) Hydroxyapatite Surfaces: A B3LYP Study

(Article begins on next page)

24 January 2022

Glycine Adsorption at Non-Stoichiometric (010) Hydroxyapatite Surfaces: a B3LYP study

Elisa Jimenez-Izal[1], Fabio Chiatti[2], Marta Corno[2], Albert Rimola[3] and Piero Ugliengo[2*]

[1]*Kimika Fakultatea, Euskal Herriko Unibertsitatea and Donostia International Physics Center (DIPC), P.K. 1072, Donostia, Euskadi, Spain*

[2]*Dipartimento di Chimica, Università degli Studi di Torino and NIS – Nanostructured Interfaces and Surfaces – Centre of Excellence, via P. Giuria 7, 10125, Torino, Italy*

[3]*Departament de Química, Universitat Autònoma de Barcelona, 08193 Bellaterra (Cerdanyola del Vallès), Spain*

[*]Corresponding author. E-mail: piero.ugliengo@unito.it

Abstract

The adsorption of glycine on the Ca-rich and P-rich HA(010) non-stoichiometric surfaces has been studied at B3LYP level using a polarized triple zeta basis set within periodic boundary conditions. Although the Ca-rich and P-rich HA(010) non-stoichiometric surfaces exhibit different terminations, giving rise to different electrostatic features in the adsorption regions, glycine preferentially adsorbs as a zwitterion on both surfaces. When adsorbed in a canonical form the proton of the COOH group is always transferred to the HA(010) surface but for one case, which, in turn, is also the least stable one. Glycine adsorbs by favorable electrostatic interactions between COO^-/Ca^{2+} and NH_3^+/PO_4^{2-} species, while dispersion interactions play a minor role. The harmonic B3LYP vibrational spectrum is in very good agreement with the experimental one and, when merged with contributions due to glycine adsorbed on stoichiometric HA(010) surfaces, allows to explain the origin of the "squat shape" of the COO^- stretching band centered at about 1600 cm^{-1}. The comparison also highlights that the Ca-rich rather than the P-rich termination, is the most suitable to explain subtle features of the experimental spectrum.

Introduction

In the latest years, calcium phosphates have been deeply studied both theoretically and experimentally because of their interesting properties and peculiarities. One of these materials is hydroxyapatite (HA, $Ca_{10}(PO_4)_6(OH)_2$), that has a special relevance because it constitutes the majority of the mineral phase of bones and tooth enamels within the human body.[1] It is used as a synthetic biomaterial because of its biocompatibility and its ability to associate with molecules, ions and metals.[2,3] For these reasons, the interaction of HA with biological molecules is of fundamental interest.

Much work has already been done concerning the characterization of HA and its interaction with molecules and ions.[4-8] In this vein, a B3LYP characterization of HA bulk and surfaces has been conducted and has confirmed the ionic nature of this material, which indeed displays a strong affinity towards polar molecules.[4,9] From previous results, the two most relevant surfaces of HA are found to be the (001) and the (010), in terms of exposure in the crystalline habit. The crystal growth occurs along the c axis during the bio-mineralization process, with the {010} crystal habit becoming the dominant one. The {010} crystal plane family can be represented by the repeating sequence …A-B-A-A-B-A-A-B-A-….,[10] in which the A and B layers have the $Ca_3(PO_4)_2$ and $Ca_4(PO_4)_2(OH)_2$ chemical compositions, respectively. For a slab of a given thickness, the most exposed layers result as ...-A-B-A, ...-A-A-B or ...-B-A-A giving rise to one stoichiometric and two non-stoichiometric HA(010) surfaces. In this particular case, the concept of stoichiometric surface refers to slabs whose chemical composition can be expressed as an integer number of $Ca_{10}(PO_4)_6(OH)_2$ formula units (2A+B) of the bulk hydroxyapatite from which they derive. The ...-A-B-A HA(010) termination exhibits the same bulk composition and the same Ca/P ratio of 1.67 of the bulk HA. The ...-A-A-B and ...-B-A-A terminations exhibits a Ca/P ratio of 1.71 and 1.63, and are consequently named as Ca-rich and P-rich, respectively.[11] Experimentally, Sato et al.[12] showed by HRTEM that the (010) surface exhibits the three different terminations, as also recently remarked by Ospina *et al*. ,[13] even if they did not analyze the detailed features of the terminations. The theoretical modeling of the

two non-stoichiometric HA(010) surfaces has already been performed by Astala and Stott with the PBE functional and the SIESTA program, also showing different behavior of these surfaces with respect to water adsorption.[7] We have recently extended the study of these surfaces, both free and when interacting with water using the B3LYP functional, showing that the Ca-rich surface is more reactive than the P-rich towards water and that, at variance with the HA(010) stoichiometric surface, water does not dissociate upon adsorption at the surface[14] in agreement with the Astala's findings.

Recently, infrared measurements of the adsorption of glycine to hydroxyapatite by chemical vapor deposition (*i.e.* in gas phase) have been reported by some of us.[15] In that work, the experimental IR spectrum was rationalized by comparison with B3LYP spectra derived from glycine adsorbed on the stoichiometric HA(010) surfaces (both pristine and water reconstructed). The conclusion was that three different glycine/HA adducts were needed in order to reproduce the "squat shape" due to the COO^- stretch band centered at 1600 cm^{-1} together with other spectral features within the 1300-1700 cm^{-1} range. Despite the good agreement between theory and experiment, the work did not consider the role of non-stoichiometric (010) HA surfaces, which, in fact, play a significant role in the HA terminations and surface exposure.[12,13]

Here we extend that work by characterizing the adsorption of glycine on the two non-stoichiometric HA(010) surfaces[5] in order to see whether the resulting IR spectra would improve or not that computed considering the stoichiometric HA(010) surfaces only. We adopted the same periodic approach in which the quantum mechanical problem was solved using localized Gaussian basis function (in this case a polarized triple-ζ all-electron basis set) more flexible than those adopted in the past and the same hybrid B3LYP functional which guarantee good accuracy in structures, energetic and vibrational features. Glycine was adsorbed either as a zwitterion or in its canonical form, to characterize adduct structures, interaction energies and vibrational features. Previous works by some of us[5,6] already proved this simple model to be useful for providing interesting clues about the behavior of more complex peptides.[16]

Computational details

The interaction between non-stoichiometric HA(010) surfaces with glycine molecules was simulated using the CRYSTAL09 periodic code.[17] Graphical manipulations have been carried out with the molecular graphics programs VMD[18] and MOLDRAW.[19]

Basis set

The multi-electron wave function was described by linear combination of crystalline orbitals which, in turn, were expanded in terms of Gaussian-type basis set functions. In previous papers, a double-ζ basis set was used along with a pseudopotential for the core electrons of Ca atom.[5] In that case, the BSSE was very large, around 45% of the interaction energy. Aiming at its reduction, in the present work we have improved the quality of the basis set: Ca atoms were described with a triple-ζ valence all-electron basis set, 86-811G(3d), with $\alpha_{sp} = 0.295$ bohr^{-2} as the exponent of the most diffuse shell and $\alpha_{pol} = 0.3191$ bohr^{-2} for polarization. A 85-21G(d) basis set was used for P atoms, with $\alpha_{sp} = 0.1350$ bohr^{-2} as the most diffuse shell exponent and $\alpha_{pol} = 0.7458$ bohr^{-2} for polarization. C atoms were represented with a 511111-411G(d) basis set (VTZ), with $\alpha_{sp} = 0.1008$ bohr^{-2} as the most diffuse shell exponent and $\alpha_{pol} = 0.8000$ bohr^{-2} for polarization.[20] N atoms were represented with a 511111-411G(d) basis set (VTZ), with $\alpha_{sp} = 0.1430$ bohr^{-2} as the most diffuse shell exponent and $\alpha_{pol} = 1.0000$ bohr^{-2} for polarization.[20] O atoms were represented with a 511111-411G(d) basis set (VTZ), with $\alpha_{sp} = 0.1751$ bohr^{-2} as the most diffuse shell exponent and $\alpha_{pol} = 0.1200$ bohr^{-2} for polarization.[20] H atom was described with a 31G(p) basis set, with $\alpha_{sp} = 0.1613$ bohr^{-2} as the most diffuse shell exponent and $\alpha_{pol} = 1.100$ bohr^{-2} for polarization. It has been demonstrated that, for systems treated within the same computational approach, the adopted polarized VTZ basis set for the atoms of the adsorbate species reduces significantly the BSSE of the computed adsorption energies, as it will be the case also here (*vide infra*).

Hamiltonian and geometry optimization

All calculations were performed within the Density Functional Theory (DFT) framework with the B3LYP hybrid functional. This functional has already been adopted by some of us,

providing results in good agreement with the experimental data.[11,21,22] The Hamiltonian matrix was diagonalized on 4 k-points. Default values of the tolerances controlling the accuracy of the Coulomb and exchange series were adopted. Atomic coordinates optimization was performed *via* an analytical gradient method, upgrading the numerical Hessian with the Broyden-Fletcher-Goldfarb-Shanno algorithm.[17]

Adsorption energies

The scheme to compute the adsorption energies is the one described by some us for similar systems.[23] A more delicate point is the evaluation of the basis set superposition error (BSSE) when adsorbates dissociate upon adsorption as happens here for glycine which loses one proton towards the HA surface. In the past we refrained to compute the BSSE corrections for technical reasons: as glycine loses its proton towards the HA surface the two separate moieties (the deprotonated glycine and the protonated HA surface) are charged, hindering the possibility of running periodic calculations at least with CRYSTAL09. In the present case, we consider the proton attached to the HA surface from the deprotonated glycine as still part of glycine. In this way, each moiety remains neutral and the periodic evaluation of the various sub-terms concurring to define the final ΔE^C value are feasible (see Table 2).[23] The procedure is internally consistent giving sensible values for the BSSE (*vide infra*), so that we propose to adopt this approach also for future work. On the fully optimized B3LYP geometries, a single point evaluation of the contribution due to dispersion interactions has been computed by means of the Grimme's method[24] available in CRYSTAL09. As dispersion is evaluated on B3LYP structures its role is expected to be somewhat underestimated compared to a full B3LYP-D optimization.

Central zone phonon frequencies

Vibrational frequencies, restricted to the glycine fragment only, were computed at the Γ point within the harmonic approximation by obtaining the eigenvalues from diagonalization of the mass-weighted Hessian matrix.[25] This strategy has been validated by some of us in the past[26]

and already adopted in some previous works on Gly adsorption.[27] The infrared intensity for each normal mode were computed using the Berry phase approach.[28] A further check on the dependence of the frequencies and infrared intensities on the fragment size was studied by including in the fragment definition also the HA surface atoms first neighbor of glycine; results show negligible variations of both observables compared to the smallest glycine fragment. The assignment of the normal modes of interest in terms of internal coordinates variations has been carried out by visual inspection of the modes using the MOLDRAW graphic program[19] and by the potential energy distribution analysis as provided by CRYSTAL09. The final B3LYP infrared spectra have been built by scaling the harmonic frequencies by a single scale factor of 0.9818, which brings the B3LYP vibrational frequencies of glycine into very good correspondence with the experimental ones for glycine entrapped in a cold Ar matrix.[29] This also allows a direct comparison with previous B3LYP spectra computed with a basis set of polarized double-zeta quality.[15] Simulated IR spectra were built by assigning a Lorentzian function with a 30 cm^{-1} width at half maximum to each vibrational frequency.

Results and discussion

Structures and interaction energy of glycine/HA(010) adducts

Previous work by some of us dealt with glycine interacting with the HA(001) and the stoichiometric HA(010) surfaces with a basis set of polarized double-zeta quality with the electron core of Ca ions described by a pseudo-potential.[5,6] For the stoichiometric HA(010) surface represented by the termination ...-A-B-A (*vide supra*) both the pristine and the water reconstructed cases were studied. Here, we extend that work by adopting an all-electron basis set of polarized triple-zeta quality and by focusing on the pristine non-stoichiometric HA(010) Ca-rich and P-rich surfaces, respectively. The non-stoichiometric HA(010) surfaces do not reconstruct by water adsorption,[14] as it was the case with the stoichiometric HA(010) one.

To study the dependency of the results obtained with the current basis set with our previous ones,[5] we have focused on one specific case, *i.e.* glycine on the HA(001) surface, by re-optimized the most stable adduct (Fig. 1). Table 1 shows the resulting energetic and geometric features. The Ca$\cdots$O bond distances only change slightly due to improvement in the basis set, whereas the NH$\cdots$O distances are more affected. In particular, the one labeled as "a" becomes shorter while "b" becomes longer by the same amount than the values computed with the double-zeta basis set. The deformation energies for slab and glycine have only a moderate dependency on the quality of the basis set, at variance with both ΔE and ΔE^* due to a different BSSE. Indeed, the BSSE becomes half of that associated with the smaller basis set and after correction, the ΔE^C and the ΔE^{*C} for different basis set become very close to each other. This data shows that both structures and interaction energies (once corrected for BSSE) are close for the two basis sets so that comparison between present and old data is feasible.

For the two new non-stoichiometric HA(010) surfaces, the atomic positions were relaxed keeping the cell vectors fixed at the B3LYP optimized HA bulk geometry, *i.e.* a = 6.854 Å, b = 9.635 Å, γ = 90.0°. This strategy enforces the underneath bulk constraints to the exposed surfaces. The slab thickness is about 20 Å for both surfaces which ensures a good representation of the chemical environment of the surface atoms with the Ca-rich and P-rich slab compositions of 4A+3B and 6A+2B units, respectively (see Fig. 2). The chosen A-A-B$\cdots$ sequence ensures that both slabs are electro neutral and nonpolar. The models are genuine 2D slabs as CRYSTAL09 does not require the definition of a fictitious empty space at the top/bottom of the considered slab, at variance with plane waves based codes. The surface electrostatic potential maps mapped on surfaces enclosing 90% of the electron density (Fig. 2) reveal a larger nucleophilic character for the Ca-rich surface, so that a large reactivity towards adsorption of electron rich molecules is expected. Each surface exhibits in the unit cell three kinds of Ca ions. For the P-rich surface the surrounding of the Ca ions is similar enough that they are almost equivalent. On the contrary, the Ca-rich surface exhibits a Ca$_3$ ion more exposed than the other two Ca cations. Since it has

already been demonstrated that the exposure of the Ca ions drives the strength of the interaction energy with respect to adsorbates, a higher reactivity is expected for the Ca-rich surface than for the P-rich one.[4,30]

A rather detailed search was done to sample all possible ways in which glycine, either in its canonical or as a zwitterion, can interact with the two HA(010) surfaces. Fig. 3 and Table 2 show the structures and energetic data, respectively. This was achieved exploiting electrostatic complementarity between the electric features of the HA(010) (see Fig. 2) surfaces and that of glycine, either in its canonical or zwitterionic forms. Data of Table 2 reveal large and negative (attraction) values for the component of the interaction energy ΔE^* free from the deformation cost and negligible lateral Gly...Gly interactions (ΔE_L^C). The deformation term of glycine is very large for all cases, for the way in which the adsorbed moiety and the perturbed HA surfaces have been treated (see Computational section for details). For instance, as glycine is always considered as a single moiety despite the transfer of its acidic proton to the HA surface, the deformation ΔE^G term can be very large as the proton may be rather far from the $NH_2CH_2COO^-$ moiety (see Fig. 3). The same happens for the HA deformation term δE_S, as the surface geometry is strongly perturbed by the presence of a proton coming from the adsorbed glycine. Both terms are computed taking as a reference energies of the structure of free glycine in its canonical form and the free relaxed HA(010) Ca-rich and P-rich slabs, respectively. The dispersion contribution (ΔE^D) is relatively small and rather constant across the considered structures (in the 45-70 kJ mol^{-1} range). As expected, the BSSE is considerably smaller than the one computed with smaller basis sets adopted by some of us for modeling water[21] and glycine[5,6] adsorption on HA surfaces.

When adsorbed as zwitterion, the most stable adduct is the Ca-r/Gly-z1 (Fig. 3, left column, top), in which the COO^- and NH_3^+ groups interact electrostatically with the surface Ca ions and by two very short H-bonds with the phosphate oxygen atoms, respectively. Interestingly, a structure (Ca-r/Gly-z1*) in which one proton of the NH_3^+ group is transferred to the P=O group was also found to be practically degenerate with the Ca-r/Gly-z1 one (see Fig. 3

and Table 2). The Ca-r/Gly-z2 one is 80 kJ·mol^{-1} lower in stability than Ca-r/Gly-z1, with shorter Ca-O bonds and one proton of the NH_3^+ group transferred to an exposed phosphate ion, giving rise to a Gly$^-$/HA$^+$ ion pair.

On the P-rich surface, P-r/Gly-z1 is the most stable adduct, with two Ca-O and two H-bonds between glycine and HA, the latter slightly longer than for the Ca-r/Gly-z1 structure. The P-r/Gly-z2 structure is only 6 kJ mol^{-1} lower in stability than the P-r/Gly-z1 structure which shows a proton transfer from the NH_3^+ to the phosphate group with the remaining NH_2 group weakly interacting (N$^{...}$Ca$_1$=2.6 Å) with the Ca$_1$ ion (Fig. 3, left column, bottom).

When glycine is adsorbed in its canonical form (Fig. 3, right column), the interaction energies are considerably smaller (on an absolute scale) than for the zwitterionic cases: the most stable adducts for the Ca-rich surface, Ca-r/Gly-n1 and Ca-r/Gly-n2 (Fig. 3, right column, top) are respectively 91 and 132 kJ·mol^{-1} higher in energy than the corresponding zwitterionic cases. In the first case, the carboxylic proton is transferred to a surface PO_4 group and the POH moiety H-bonds the glycine COO$^-$ group. For Ca-r/Gly-n2, the COOH group H-bonds to the HA surface OH$^-$ ion without proton transfer towards the surface. Indeed, the OH$^-$ ion is not very reactive, as already reported in Ref.[14] This structure is also the least stable one and the various terms contributing to the final ΔE^C are much smaller (in absolute value) than for all other cases as glycine is adsorbed in its canonical form. In both adducts the N atom of the NH_2 group and the O atom of the C=O group weakly interact with surface Ca ions.

For the P-rich surface the adsorption of glycine in its canonical form is always weaker compared to the zwitterionic cases (Fig. 3, right column, bottom), as already found for the Ca-rich surface. For both P-r/Gly-n1 and P-r/Gly-n2 proton transfer does occur and the oxygen atoms of the COO$^-$ group interact either with a different Ca ion or in a bi-dentate fashion.

The present results reveal that HA(010) non-stoichiometric surfaces are less reactive towards glycine than the corresponding stoichiometric one. As an indication of that, glycine transfers, in all cases, the COOH acidic proton to the stoichiometric HA(010) surface.[5] Unexpectedly, the chemical behavior of the non-stoichiometric HA(010) surfaces is closer to the

HA(001) surface, where the dissociation does not occur for the most stable zwitterionic/surface adduct, occurring instead for glycine adsorbed in its canonical form.[5]

Vibrational features of glycine/HA(010) adducts

Very recently a comparison between the experimental infrared spectra of glycine adsorbed from chemical vapor deposition to hydroxyapatite nanocrystals and the B3LYP one have been carried out.[15] The interaction of glycine with HA(001) and stoichiometric HA(010) surfaces was considered in order to account for the subtle experiment spectral features recorded in the 1300-1700 cm^{-1} region. In particular, the most striking feature was the "squat shape" of the most intense band around 1600 cm^{-1} (see Fig. 5 or Ref.[15]) due to the COO$^-$ stretching modes, which was interpreted as the convolution of bands from different glycine adducts on both the HA(010) and the water reacted HA(010)w surface. That study also excluded contributions to the spectra from glycine adsorbed on the HA(001) surface. To further disentangle the contributions of both COO$^-$ and CCH modes from that due to NH and OH modes, isotopic H/D substitution was carried out for protons of the COOH and NH$_2$ groups for both experiment and computational setup. In the 1300-1700 cm^{-1} region, the bands originate from both symmetric ν(COO$^-$)s stretching and bending δ(CCH) modes, which are usually also coupled.

The previous paragraph reports nine different potential structures for which the infrared spectra have been computed. To screen them out, we have adopted a Boltzmann's weighting scheme based on the relative adsorption energies. In this way, the only contributing spectra are those for Ca-r/Gly-z1, Ca-r/Gly-z1*, P-r/Gly-z1 and P-r/Gly-z2 structures, the spectra being built as Boltzmann's weighted linear combinations of single components and resulting as: 0.17*Ca-r/Gly-z1+0.83*Ca-r/Gly-z1 and 0.92*P-r/Gly-z1+0.08*P-r/Gly-z2, respectively. Fig. 4a shows B3LYP spectra for the separate Ca-rich and P-rich structures together with the resulting spectrum obtained by the Boltzmann weighted sum. Comparison with the experimental spectrum[15] (full discussion on the assignment of the bands is described in the same reference) reveals an excellent agreement as far as the ν(COO$^-$) asymmetric stretch around 1600 cm^{-1} as

well as the complex band located in the 1450-1400 cm^{-1} region due to the coupling between the symmetric $\nu(COO^-)$ stretch and the $\delta(CCH)$ deformation mode. In Fig. 4b the resulting B3LYP spectrum from the non-stoichiometric HA(010) surfaces is merged with that previously computed for the stoichiometric HA(010) ones (IR intensities have been scaled by 1.19 scale factor to account for the different basis set adopted in Ref.[15]). The agreement with the experimental spectrum of Fig. 4c is striking which proves the role of the non-stoichiometric Ca-rich and P-rich HA(010) surfaces as important structural features of the hydroxyapatite nanocrystals morphology. From the merged spectra it clearly turned out that the "squat shape" of the COO$^-$ stretch band is due to a multicomponent contribution from different glycine adducts on both stoichiometric and non-stoichiometric HA(010) faces. As the band around 1320 cm^{-1} is only present in the spectrum computed for the Ca-rich HA(010) structures as well as a more structured one at around 1420 cm^{-1}, it indicates this termination as more relevant over the P-rich one on the non-stoichiometric HA(010) faces of the nanocrystals.

It is worth noting that when we analyzed the separate IR spectrum for each of the structures of Fig. 3 it turned out that the Ca-r/Gly-z1 spectrum shows a strong component in the 1500 cm^{-1} region, completely absent in the experiment (see Fig. 4). Inspection of the mode revealed that the band is due to N-D stretch modes associated to the strong and almost symmetric H-bonds between the ND$_3^+$ group and the P=O groups (distance of ~1.4 Å, see Fig. 3): the bathochromic N-D stretching frequency shifts is so large that the N-D mode shows up as a very intense band at 1500 cm^{-1}. Extreme caution should however be taken in such cases before giving credit to the computed results. Indeed, large amplitude motion associated to the deuterium atom involved in strong H-bond implies that the harmonic treatment is inadequate and also density functional theory in the present form may show some weakness when dealing with low energy barrier for proton motion. Furthermore, Fermi resonance is possible between the shifted N-D stretching modes and other modes in the same region giving rise to complex spectral features like the Evans windows, as described for strong H-bonds between probe molecules in acidic zeolites.[31,32] Therefore, the present harmonic treatment, for this case, cannot describe these

complex spectral features. For these reasons, we cannot trust the prediction of this particular band in the B3LYP spectrum so that we pragmatically removed it from the set of frequencies leaving all other modes unaltered as they do not suffer from the limitations of the harmonic treatment. This problem does not occur for any of the considered structures, not even for the closest Ca-r/Gly-z1* structure in which the proton of the NH_3^+ group is transferred to the P=O group with consequent longer (and weaker) H-bonds.

Conclusions

In the present work, the adsorption of glycine on the non-stoichiometric HA(010) surfaces has been studied at B3LYP level using a polarized triple-zeta basis set adopting periodic boundary conditions to model the interaction. The Ca-rich and P-rich non-stoichiometric HA(010) surfaces exhibit different terminations giving rise to distinct electrical features which differentiate the glycine adsorption. At variance with the reactivity of the HA(001) surface, glycine preferentially adsorbs as a zwitterion on both Ca-rich and P-rich surfaces. The stabilization is due to favorable electrostatic interactions between COO^-/Ca^{2+} and NH_3^+/PO_4^{2-} species, while dispersion interactions are playing a less relevant role. Of the two non-stoichiometric surfaces the Ca-rich one appears to be the more reactive than the P-rich. The harmonic B3LYP vibrational spectrum has been constructed by considering a Boltzmann's weighted sum based on relative stability of the spectra for each of the nine structures resulted from geometry optimization. The agreement between the bands details of the experimental spectrum and the one simulated at B3LYP level is very good when the IR bands from the present calculations on the non-stoichiometric HA(010) surfaces are merged with the previous one on the stoichiometric HA(010) ones.[15] The final spectrum completely accounts for the origin of the "squat shape" of the band centered at about 1600 cm^{-1} due to the COO^- stretching mode of the adsorbed glycine and of the rather broad feature around 1420 cm^{-1}. For this latter, in particular, the Ca-rich termination provides a more convincing comparison with the experimental spectrum with respect to the P-rich termination.

Acknowledgements

Table 1. Energetic features (the apex C means BSSE corrected value) of the glycine adsorption on the (001) HA surface as a function of the basis set quality. ΔE is the final interaction energy, ΔE^* the deformation free interaction energy, δE_S and δE_G the HA(010) surface deformation energy and the glycine deformation energy plus the glycine lateral interactions ΔE_L, respectively. Energetic data in kJ mol^{-1}, distances in Å.

Energy	δE_S	δE_G	ΔE_L	ΔE^*	ΔE^{*C}	ΔE	ΔE^C	%BSSE
Double-ζ	52	118	-23	-418	-306	-248	-136	45
Triple-ζ	81	104	-24	-343	-315	-158	-130	18
Geometry		Ca1-O1		Ca3-O2		a		b
Double-ζ		2.334		2.354		1.622		1.956
Triple-ζ		2.382		2.342		1.671		1.901

Table 2. Energetic features (the apex C means BSSE corrected value) of the interactions between glycine and HA(010) non-stoichiometric surfaces (Ca-r(ich) and P-r(ich)). δE_S and δE_G are the HA(010) deformation energy and the sum of molecular glycine deformation, ΔE_G, and the glycine lateral interactions, ΔE_L. ΔE is the interaction energy, ΔE^* is the interaction energy free from the cost of deformation, ΔE^D is the pure dispersive contribution, calculated *a posteriori* with the Grimme's correction which is added to the ΔE^C to give the final ΔE^{CD}. Data in kJ mol^{-1}.

Structure	δE_S	δE_G	ΔE_G	$\Delta E_L{}^C$	ΔE^*	ΔE^{*C}	ΔE	ΔE^C	BSSE(%)	ΔE^D	ΔE^{CD}
HA (010) Ca-rich											
Ca-r/Gly-z1	91	144	164	-20	-527	-496	-292	-262	10	-59	-321
Ca-r/Gly-z1*	117	321	341	-19	-729	-697	-291	-258	11	-59	-317
Ca-r/Gly-z2	98	282	309	-27	-605	-575	-225	-195	13	-46	-241
Ca-r/Gly-n1	145	449	449	0	-812	-780	-216	-185	15	-45	-230
Ca-r/Gly-n2	36	28	30	-2	-222	-197	-157	-132	16	-57	-190
HA (010) P-rich											
P-r/Gly-z1	107	140	152	-13	-509	-473	-263	-227	14	-61	-288
P-r/Gly-z2	244	693	711	-18	-1196	-1149	-258	-212	18	-70	-282
P-r/Gly-n1	161	588	587	0	-972	-940	-223	-191	15	-59	-250
P-r/Gly-n2	221	670	686	-16	-1111	-1067	-220	-176	20	-61	-236

Captions to the Figures

Figure 1. Local view of glycine adsorbed on the HA(001) surface.

Figure 2. Left column: lateral view of the HA(010) Ca-rich and P-rich slabs. A: $Ca_3(PO_4)_2$; B: $Ca_4(PO_4)_2(OH)_2$. Right column: top view of the Ca-rich and P-rich surfaces, superimposed to the electron isodensity (ρ) surface color coded by the B3LYP electrostatic potential (V) values. $\rho = 10^{-6}$ a.u., V from -0.02 a.u. (red) to 0.02 a.u. (blue).

Figure 3. B3LYP optimized geometries and interaction energies (Table 2) of glycine adsorbed on HA(010) Ca-rich and P-rich surfaces, respectively.

Figure 4. Section a): B3LYP spectra of glycine adsorbed on the non-stoichiometric HA(010) Ca-rich and P-rich surfaces. Dotted blue curve: 0.92*P-r/Gly-z1+0.08*P-r/Gly-z2; Dashed red curve: Ca-rich: 0.83*Ca-r/Gly-z1+0.17*Ca-r/Gly-z1*; Black line: sum of the two spectra; Section b): B3LYP spectra of glycine adsorbed on the non-stoichiometric HA(010) Ca-rich and P-rich surfaces and on the stoichiometric (010) ones. Dotted blue curve: Gly on stoichiometric Gly/HA(010) surfaces (see Ref. [15]); Dashed green curve: Gly on non-stoichiometric HA(010) surfaces (see black line of Section a); Black curve: sum of the two spectra; EXP: experimental spectrum recorded after chemical vapour deposition of Gly on HA nanocrystals[15]. B3LYP frequencies have been scaled by 0.9818 factor.
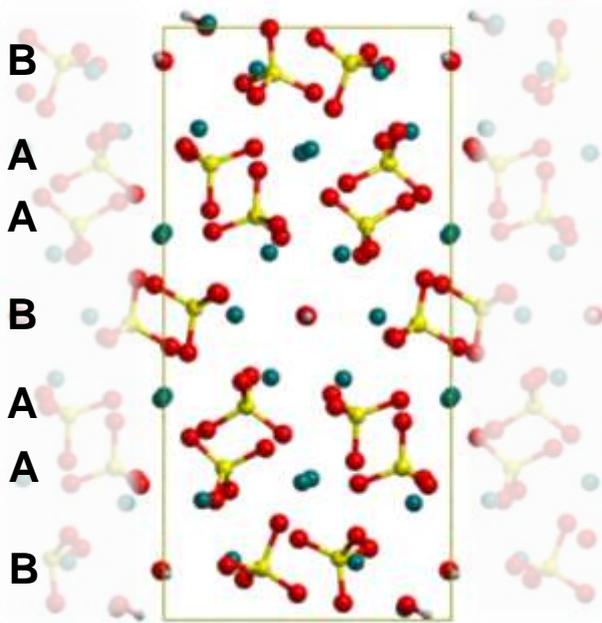
(001)/Gly-z
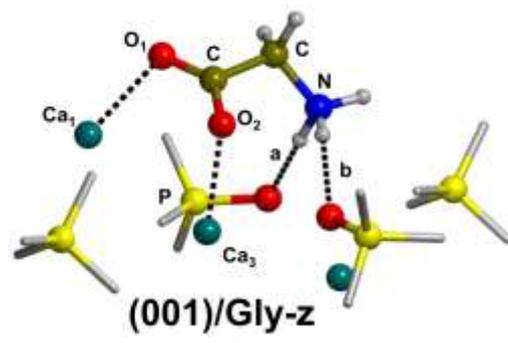
Figure 1

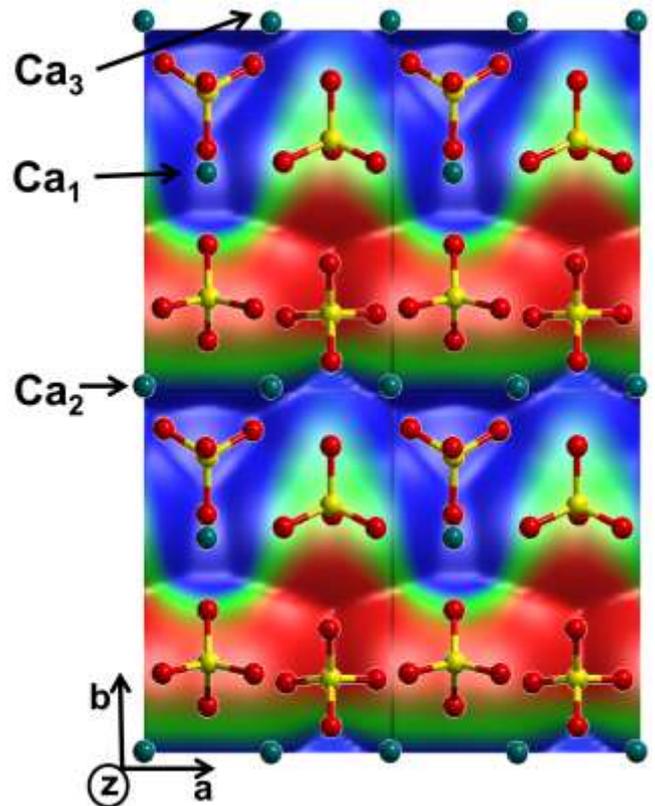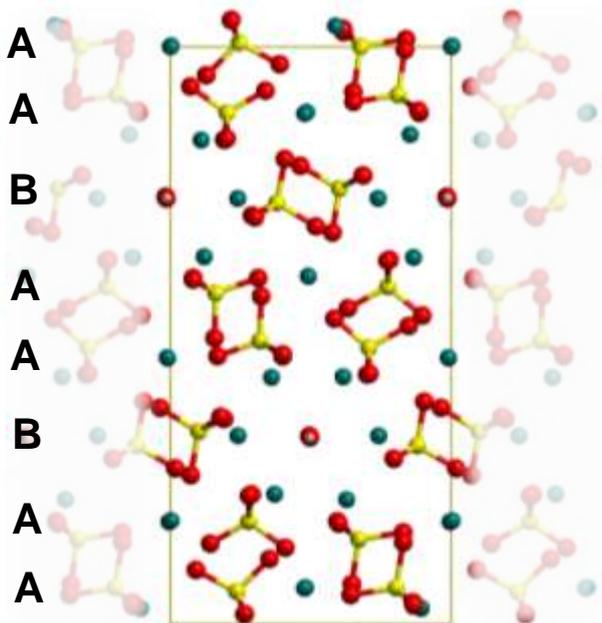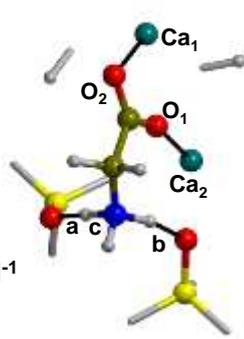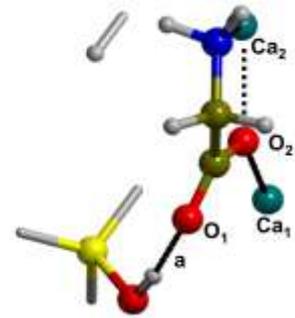# Ca-rich HA(010)
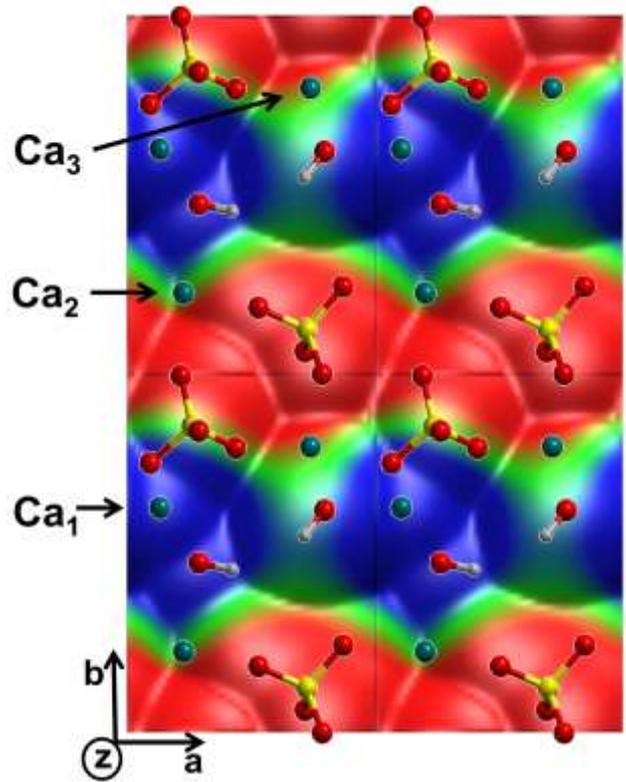
P-rich HA(010)

Figure 2

Ca₁-O₂: 2.521 [2.467] Å

Ca₂-O₁: 2.369 [2.348] Å

a: 1.415 [1.073] Å

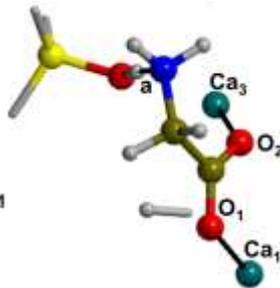b: 1.674 [1.951] Å

c: 1.120 [1.492] Å

ΔE = -321 [-317] kJ mol⁻¹

Ca-r/Gly-z1
[Ca-r/Gly-z1*]

Ca₁-O₂: 2.405 Å

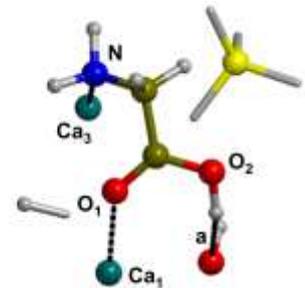Ca₃-O₂: 2.422 Å

Ca₁-N: 2.599 Å

a: 1.730 Å

ΔE = -230 kJ·mol⁻¹

Ca-r/Gly-n1

Ca₁-O₁: 2.378 Å

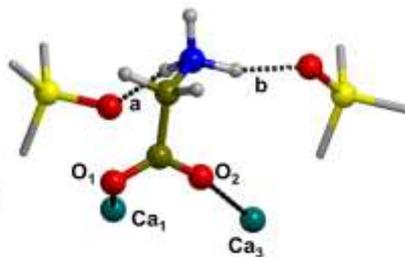Ca₃-O₂: 2.357 Å

a: 1.464 Å

ΔE = -241 kJ·mol⁻¹

Ca-r/Gly-z2

Ca₁-O₁: 2.330 Å

Ca₃-N: 2.601 Å
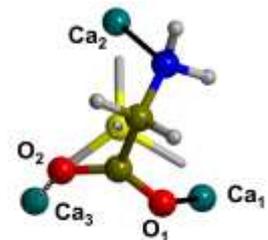
a: 1.792 Å

ΔE = -190 kJ·mol⁻¹

Ca-r/Gly-n2

Ca₁-O₁: 2.562 Å

Ca₃-O₂: 2.237 Å

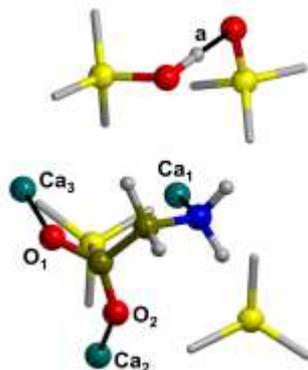a: 1.748 Å

b: 1.691 Å

ΔE = -288 kJ·mol⁻¹

P-r/Gly-z1

Ca₃-O₂: 2.322 Å

Ca₁-O₁: 2.375 Å
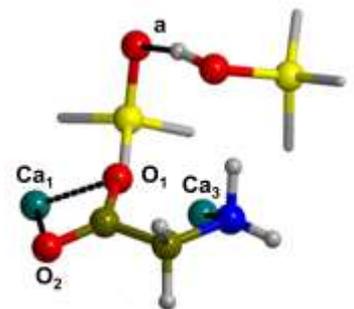
Ca₂-N: 2.623 Å

ΔE = -250 kJ·mol⁻¹

P-r/Gly-n1

Ca₂-O₂: 2.315 Å

Ca₃-O₁: 2.300 Å

Ca₁-N: 2.589 Å

O-H: 0.989 Å

a: 1.927 Å

ΔE = -282 kJ·mol⁻¹

P-r/Gly-z2

Ca₁-O₁: 2.350 Å

Ca₁-O₂: 2.310 Å

Ca₃-N: 2.676 Å

a: 1.865 Å

ΔE = -236 kJ·mol⁻¹

P-r/Gly-n2

Figure 3

a — B3LYP

b — B3LYP

c — EXP

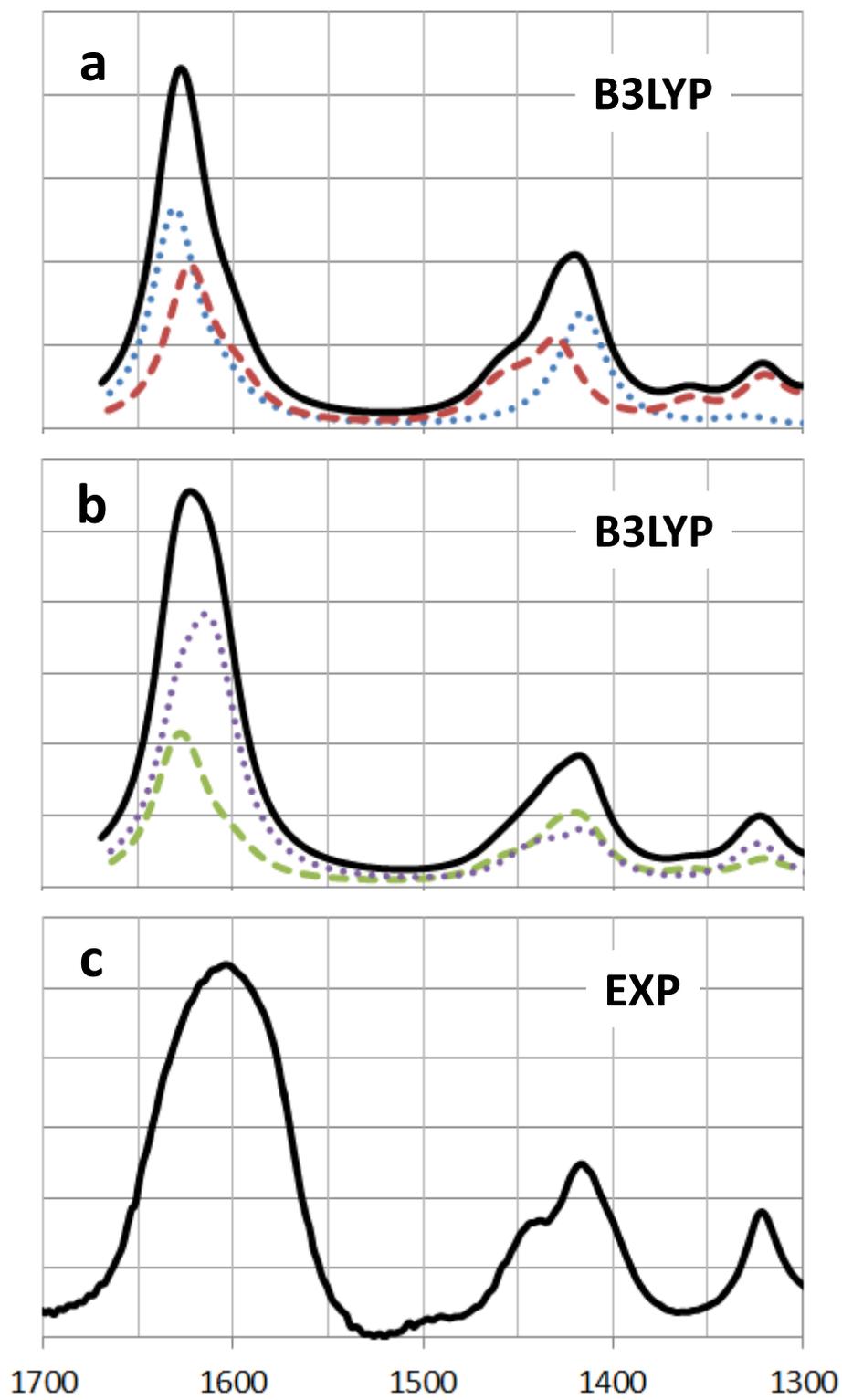1700   1600   1500   1400   1300

Figure 4

Bibliography

(1)   Young, R. A.; Brown, W. E. Structures of Biological Minerals. In *Biological Mineralization and Demineralization*; Nancollas, G. H., Ed.; Springer-Verlag: Berlin, Heidelberg, New York, 1982; pp 101-141.

(2)   Habraken, W. J. E. M.; Wolke, J. G. C.; Jansen, J. A. *Adv. Drug. Deliver. Rev.* **2007**, *59*, 234-248.

(3)   Vallet-Regì, M.; Gonzàlez-Calbet, J. M. *Prog. Solid State Chem.* **2004**, *32*, 1-31.

(4)   Corno, M.; Rimola, A.; Bolis, V.; Ugliengo, P. *Phys. Chem. Chem. Phys.* **2010**, *12*, 6309-6329.

(5)   Rimola, A.; Corno, M.; Zicovich-Wilson, C. M.; Ugliengo, P. *J. Am. Chem. Soc.* **2008**, *130*, 16181-16183.

(6)   Rimola, A.; Corno, M.; Zicovich-Wilson, C. M.; Ugliengo, P. *Phys. Chem. Chem. Phys.* **2009**, *11*, 9005-9007.

(7)   Astala, R.; Stott, M. J. *Phys. Rev. B* **2008**, *78*, 075427-075437.

(8)   Almora-Barrios, N.; de Leeuw, N. H. *CrystEngComm* **2010**, *12*, 960-967.

(9)   Rimola, A.; Corno, M.; Garza, J.; Ugliengo, P. *Phil. Trans. R. Soc. A* **2012**, *370*, 1478-1498.

(10)   Sato, K.; Kogure, T.; Kumagai, Y.; Tanaka, J. *J. Colloid. Interf. Sci.* **2001**, *240*, 133-138.

(11)   Corno, M.; Chiatti, F.; Pedone, A.; Ugliengo, P. In Silico Study of Hydroxyapatite and Bioglass®: How Computational Science Sheds Light on Biomaterials. In *Biomaterials - Physics and Chemistry*; Pignatello, R., Ed.; InTech, 2011; pp 275-298.

(12)   Sato, K.; Kogure, T.; Iwai, H.; Tanaka, J. *J. Am. Ceram. Soc.* **2002**, *85*, 3054-3058.

(13)   Ospina, A.; Terra, J.; Ramirez, A. J.; Farina, M.; Ellis, D. E.; Rossi, A. M. *Coll. Surf. B* **2012**, *89*, 15-22.

(14)   Chiatti, F.; Corno, M.; Bolis, V.; Ugliengo, P., *in preparation*.

(15)   Rimola, A.; Sakhno, Y.; Bertinetti, L.; Lelli, M.; Martra, G.; Ugliengo, P. *J. Phys. Chem. Lett.* **2011**, *2*, 1390-1394.

(16)   Rimola, A.; Aschi, M.; Orlando, R.; Ugliengo, P. *J. Am. Chem. Soc.* **2012**, *Just Accepted Manuscript*, DOI: 10.1021/ja302262y.

(17)   Dovesi, R.; Saunders, V. R.; Roetti, C.; Orlando, R.; Zicovich-Wilson, C. M.; Pascale, F.; Civalleri, B.; Doll, K.; Harrison, N. M.; Bush, I. J.; D'Arco, P.; Llunell, M.; University of Turin: CRYSTAL2009 User's Manual. Turin, 2009.

(18)   Humphrey, W.; Dalke, A.; Schulten, K. *J. Molec. Graphics* **1996**, *14*, 33-38.

(19)   Ugliengo, P.; Viterbo, D.; Chiari, G. *Z. Kristallogr.* **1993**, *207*, 9-23.

(20)   Schafer, A.; Horn, H.; Ahlrichs, R. *J. Chem. Phys.* **1992**, *97*, 2571-2577.

(21)   Corno, M.; Busco, C.; Bolis, V.; Tosoni, S.; Ugliengo, P. *Langmuir* **2009**, *25*, 2188-2198.

(22)   Corno, M.; Orlando, R.; Civalleri, B.; Ugliengo, P. *Eur. J. Mineral.* **2007**, *19*, 757-767.

(23)   Rimola, A.; Sodupe, M.; Tosoni, S.; Civalleri, B.; Ugliengo, P. *Langmuir* **2006**, *22*, 6593-6604.

(24)   Grimme, S. *J. Comput. Chem.* **2006**, *27*, 1787-1799.

(25)   Pascale, F.; Zicovich-Wilson, C. M.; Gejo, F. L.; Civalleri, B.; Orlando, R.; Dovesi, R. *J. Comput. Chem.* **2004**, *25*, 888-897.

(26)   Tosoni, S.; Pascale, F.; Ugliengo, P.; Orlando, R.; Saunders, V. R.; Dovesi, R. *Mol. Phys.* **2005**, *103*, 2549-2558.

(27)   Rimola, A.; Civalleri, B.; Ugliengo, P. *Langmuir* **2008**, *24*, 14027-14034.

(28)   Noel, Y.; Zicovich-Wilson, C. M.; Civalleri, B.; D'Arco, P.; Dovesi, R. *Phys. Rev. B.* **2001**, *65*, 014111-014120.

(29)   Stepanian, S. G.; Reva, I. D.; Radchenko, E. D.; Rosado, M. T. S.; Duarte, M.; Fausto, R.; Adamowicz, L. *J. Phys. Chem. A* **1998**, *102*, 1041-1054.

(30)   Bolis, V.; Busco, C.; Martra, G.; Bertinetti, L.; Sakhno, Y.; Ugliengo, P.; Chiatti, F.; Corno, M.; Roveri, N. *Phil. Trans. R. Soc. A* **2012**, *370*, 1313-1336.

(31)   Paze, C.; Bordiga, S.; Lamberti, C.; Salvalaggio, M.; Zecchina, A.; Bellussi, G. *J. Phys. Chem. B* **1997**, *101*, 4740-4751.

(32)   Zecchina, A.; Arean, C. O. *Chem. Soc. Rev.* **1996**, *25*, 187-197.

Graphic Table of content